



Full length article

# Functionally engineered extracellular vesicles improve bone regeneration



Chun-Chieh Huang<sup>a</sup>, Miya Kang<sup>a</sup>, Yu Lu<sup>a</sup>, Sajjad Shirazi<sup>a</sup>, Jose Iriarte Diaz<sup>a</sup>, Lyndon F Cooper<sup>a</sup>, Praveen Gajendrareddy<sup>b,\*</sup>, Sriram Ravindran<sup>a,\*</sup>

<sup>a</sup> Department of Oral Biology, College of Dentistry, University of Illinois at Chicago, Chicago, IL 60612, USA

<sup>b</sup> Department of Periodontics, College of Dentistry, University of Illinois at Chicago, Chicago, IL 60612, USA

---

## ARTICLE INFO

### Article history:

Received 20 December 2019

Revised 3 April 2020

Accepted 8 April 2020

Available online 16 April 2020

---

### Keywords:

Extracellular vesicles

Exosomes

Mesenchymal stem cells

Bone regeneration

BMP2

---

## ABSTRACT

Lineage specific differentiation of host mesenchymal stem cells (MSCs) is a necessary step for bone repair/regeneration. Clinically, growth factors such as bone morphogenetic protein 2 (BMP2) are used to enhance/hasten this process to heal critical sized defects. However, the clinical application of such growth factors is fraught with dosage challenges as well as immunological and ectopic complications. The identification of extracellular vesicles (EVs) as active components of the MSC secretome suggest alternative approaches to enhancing bone regeneration. Based on our earlier studies on the properties of EVs from lineage specified MSCs, this study sought to engineer EVs to enhance osteogenic differentiation. To generate MSC EVs with enhanced osteoinductive abilities, genetically modified human bone marrow derived MSCs (HMSCs) were generated by constitutively expressing BMP2. We hypothesized that these cells would generate functionally engineered EVs (FEEs) with enhanced osteoinductive properties. Our results show that these FEEs maintained the general physical and biochemical characteristics of naïve HMSC EVs in the form of size distribution, EV marker expression and endocytic properties but show increased bone regenerative potential compared to MSC EVs in a rat calvarial defect model *in vivo*. Mechanistic studies revealed that although BMP2 was constitutively expressed in the parental cells, the corresponding EVs (FEEs) do not contain BMP2 protein as an EV constituent. Further investigations revealed that the FEEs potentiate the BMP2 signaling cascade possibly due to an altered miRNA composition. Collectively, these studies indicate that EVs' functionality may be engineered by genetic modification of the parental MSCs to induce osteoinduction and bone regeneration.

### Significance statement

With mounting evidence for the potential of MSC EVs in treatment of diseases and regeneration of tissues, it is imperative to evaluate if they can be modified for application specificity. The results presented here indicate the possibility for generating Functionally Engineered EVs (FEEs) from MSC sources. As a proof of concept approach, we have shown that EVs derived from genetically modified MSCs (BMP2 over-expression) can be effective as biomimetic substitutes for growth factors for enhanced tissue-specific regeneration (bone regeneration) *in vivo*. Mechanistic studies highlight the role of EV miRNAs in inducing pathway-specific changes. We believe that this study will be useful to researchers evaluating EVs for regenerative medicine applications.

© 2020 Acta Materialia Inc. Published by Elsevier Ltd. All rights reserved.

---

## 1. Introduction

Bone repair and regenerative procedures are among the most frequently performed surgical procedures in the world. Recently, with the many wars around the globe, complexities arising from lifestyle related diseases such as obesity and type II diabetes and increased lifespan, the incidence of bone injuries and the need

---

\* Corresponding authors.

E-mail addresses: [praveen@uic.edu](mailto:praveen@uic.edu) (P. Gajendrareddy), [sravin1@uic.edu](mailto:sravin1@uic.edu) (S. Ravindran).

for regenerative surgeries has increased significantly [1–5]. As clinical challenges have increased, innovations in the fields of biomedical engineering and tissue engineering have continued to address these challenges. Tissue engineering strategies are based on the combined use of stem cells, scaffolds and growth factors as proposed by Langer and Vacanti [6]. The introduction of bone morphogenetic protein 2 (BMP2), a potent osteoinductive factor provided a readily available strategy to augment bone growth in combination with existing clinical bone grafting materials. BMP2 is FDA approved for delivery on a collagen scaffold and is used in many bone regenerative applications [7]. However, several clinical side effects have been reported over the years (reviewed in [8]). These include, but not limited to ectopic bone formation, inflammatory complications, neurological complications, osteoclast activation and wound site complications such as hematoma and wound dehiscence. These serious side effects have spurred research into alternative biologicals that can mitigate risks and show similar efficacy.

Stem cell therapy is an alternative that has been explored as well. Mesenchymal stem cells (MSCs) serve as an ideal choice owing to their multipotency and availability from a variety of tissue sources [9]. Indeed, MSCs have been evaluated in large animal models as well as in clinical trials for safety and efficacy and may prove to be beneficial for bone regeneration [10]. Despite this promise, MSCs face significant regulatory and logistical hurdles. Autologous use is limited by age and patient's health status followed by extensive expansion requirements and allogenic use of MSCs requires efficient screening techniques, efficacy testing and banking. Furthermore, the timing and dosage of MSCs required for treatment is still a significant knowledge gap [11].

The MSC immunomodulatory and bone regenerative function are attributable to paracrine mechanisms enacted by secreted factors [12,13]. MSC derived extracellular vesicles (EVs) have been implicated as important contributors to MSC paracrine function. When MSC EVs have been used in regenerative studies, they have performed equally to MSCs, suggesting that MSC EV are an active component of the MSC secretome during regeneration and wound healing. This highlights the potential use of EVs as an alternative or adjuvant to both stem cell and growth factor therapy [14]. We and others have demonstrated that MSC EVs possess osteoinductive properties and that EVs from differentiating MSCs and osteoblasts can induce osteogenic differentiation of naïve MSCs [15,16]. However, naïve MSC EVs are only minimally effective in promoting bone regeneration [17]. Upon osteoblastic differentiation of MSCs, their respective EVs show enhanced osteoinductive potential [15,16]. This altered functionality implies induced changes in the MSC cargo. As such, we sought to explore the potential to engineer EVs of enhanced osteoinductive function for bone regeneration by use of a cellular source representing the differentiating osteoprogenitor.

Therefore, we created a stable cellular platform to consistently produce osteoinductive MSC EVs. To achieve this, we generated human bone marrow derived MSC cells that constitutively express BMP2 and demonstrate osteoblastic differentiation to serve as a source for osteoinductive EVs. We tested the hypothesis that constitutive expression of hBMP2 in MSCs would promote the expression of functionally engineered EVs (FEEs) with enhanced osteoinductive function *in vitro* and *in vivo*.

## 2. Materials and methods

### 2.1. Cell culture

Human bone marrow derived primary MSCs (HMSCs) were purchased from ATCC and Lonza. HMSCs were cultured in  $\alpha$ MEM

(Gibco) containing 20% (v/v) fetal bovine serum (FBS, Gibco), 1% (v/v) L-Glutamine (Gibco) and 1% (v/v) antibiotic-antimycotic solution (Gibco) [18]. The multipotency of the MSCs was verified as per our published methodology for osteogenic, chondrogenic and adipogenic differentiation [19].

### 2.2. Generation and characterization of BMP2 overexpressing HMSCs (BMP2 OE HMSCs)

Lentiviral particles containing a mammalian dual promoter vector that encodes the BMP2 gene under the control of EF1 $\alpha$  promoter and a GFP marker under the control of SV40 promoter or control vector without the BMP2 gene was obtained from Applied Biological Materials (ABM). HMSCs were transfected with the lentiviral particles according to the manufacturer's instructions and stably selected using puromycin. The increase in expression of the BMP2 mRNA was verified by qRT PCR with respect to control and vector alone expressing control HMSCs. The ability of the BMP2 OE HMSCs for enhanced osteogenic differentiation was verified by subjecting 100,000 control, vector alone (no BMP2 overexpression) expressing HMSCs and BMP2 OE HMSCs to osteogenic differentiation (as per previously published protocols [19]) in 6 well tissue culture plates and subjecting them to alizarin red staining to observe differentiation-associated mineralization. EVs were isolated and characterized from these overexpressing (BMP2 FEEs) and control HMSCs as described below.

### 2.3. EV isolation and characterization

EVs were isolated from the HMSC culture medium according to established protocols [18]. Briefly, HMSCs were washed in serum free medium and cultured under serum free condition for 24 h. The culture medium was harvested and removed of cell debris by centrifugation (1500 $\times$ g) for 15 min. The medium was concentrated fivefold using a 100 KDa spin filter (Millipore) and EVs were isolated using the ExoQuick TC isolation reagent (System Biosciences) as per the manufacturer's recommended protocols. The isolated EVs were quantified using nanoparticle tracking analysis (NTA) and resuspended in PBS at a stock concentration of 100,000 particles/ $\mu$ l. The isolated EVs were characterized morphologically and by transmission electron microscopy (TEM) and biochemically by assessment of membrane markers by immunoblotting [20].

EV proteins were isolated for immunoblotting in RIPA buffer and 10–20  $\mu$ g of EV protein isolates (estimated using BCA assay (Thermo Scientific)) were resolved by SDS-PAGE and immunoblotting was performed for CD63 and CD9 markers as described previously [16,18,19]. The blots were then dried and imaged using a Licor Odyssey CLx imager. For immunoblotting of the conditioned medium from which EVs were isolated, medium was dialyzed (7.5 KDa cutoff) against deionized water for 48 h with 4 exchanges, lyophilized ( $-50^{\circ}$ C) and reconstituted in 1 $\times$  Laemmli buffer. SDS PAGE and immunoblotting was performed as described.

For transmission electron microscopy (TEM), 10 $\mu$ l of 10,000 particles/ $\mu$ l of the EV suspensions were placed on to carbon formvar-coated nickel TEM grids and incubated for 1 h followed by fixing with 4% (v/v) formalin, washing with double deionized water and air drying. For immunogold labeling of CD63, the EV containing grids were blocked in PBS with 5% BSA, incubated with CD63 antibody (1/100, Abcam) followed by washing and incubation with 10 nm gold tagged secondary antibody (1/1000, Abcam). The grids were then washed and air-dried. The prepared grids were imaged using a Joel JEM3010 TEM.

## 2.4. Quantitative and qualitative endocytosis of EVs

For endocytosis experiments, EVs were fluorescently labeled using the ExoGlow green labeling kit (System Biosciences) that labels the exosomal proteins fluorescently. For quantitative experiments, HMSC were plated in 96 well tissue culture plates at a concentration of 10,000 cells per well and incubated for 18 h to facilitate cell attachment. The cells were then incubated with increasing amounts of fluorescently labeled EVs for 2 h at 37 °C and subsequently washed with PBS and fixed in neutral buffered 4% (w/v) paraformaldehyde. The fluorescence from the endocytosed EVs was measured using a BioTek Cytation 96 well plate reader equipped with the appropriate filter sets to measure green fluorescence. The results were plotted as mean ( $\pm$  SD) normalized fluorescence intensities (normalized to background and no EV fluorescence) as a function of dosage ( $n = 6$  per group).

For quantitative endocytosis blocking experiments, the cells were plated in 96 well plates as described above or in 12 well culture plates (50,000 cells/well). Prior to EV treatment, cells were pre-treated with the blocking agents for 1 h [18]. Cell surface integrins were blocked with 2 mM RGD polypeptide (Sigma). Membrane cholesterol was depleted using methyl  $\beta$  cyclodextrin (MBCD, Sigma) in a dose dependent manner (0–10 mM). In addition to this, the labeled EVs were pretreated for 1 h with indicated concentrations of heparin (0–10  $\mu$ g/ml, Sigma) to block the heparin sulfate proteoglycan binding sites on the exosomal membrane. For the qualitative and quantitative experiments, to ensure that saturable levels of HMSC EVs were used in the assay, twice the saturable amount of EVs was used. The saturable EV amount was determined using the dose dependent endocytosis experiment. Treatment with the EV suspension was carried out as described previously and the fluorescence measurement and quantitation was performed according to previously described protocols [18].

For qualitative endocytosis experiments, 50,000 cells (HMSCs) were plated on coverslips placed in 12 well tissue culture dishes. Fluorescently labeled EVs at 2 $\times$  saturation were then added with/without inhibitors as described above and incubated for 2 h in the presence/absence of blocking agents as described above. The treated HMSCs were then washed, fixed in 4% (w/v) neutral buffered paraformaldehyde, permeabilized and counter stained using mouse monoclonal anti tubulin antibody (1/2000, Sigma), rabbit polyclonal anti caveolin1 antibody (1/100, Santa Cruz Biotechnology) or rabbit polyclonal anti clathrin antibody (1/100, Santa Cruz Biotechnology) followed by treatment with TRITC labeled anti mouse/rabbit secondary antibody. The coverslips were then mounted using mounting medium containing DAPI (Vector Labs) to label the nuclei and imaged using a Zeiss LSM 710 Meta confocal microscope.

## 2.5. EV mediated HMSC differentiation

For *in vitro* differentiation experiments, HMSCs (250,000 cells per 1cm $\times$ 1cm collagen sponge) were cultured within type I collagen sponges (Zimmer collagen tape) in quadruplicate. 1  $\times$  10 $^8$  BMP2 FEE particles was used per group in this experiment (2 $\times$  saturation). Untreated cells received PBS treatment of equal volumes and incubated for 72 h. Post 72 h, RNA was isolated from the embedded HMSCs followed by cDNA synthesis and qRT PCR for selected osteoinductive marker genes as per our previously published protocols and primer sequences [16,18,19].

## 2.6. SMAD 1/5/8 pathway studies

For the reporter assay, 30,000 HMSCs cultured in 24 well tissue culture plates were transfected in quadruplicate with control

or SMAD 1/5/8 specific luciferase reporter plasmid (SBE12 [21]) using lipofectamine transfection reagent [21]. Forty-eight hours post transfection, the cells were treated with the control or experimental reagents in quadruplicate. The EVs were added at 2 $\times$  saturation as described previously. This amounted to 6  $\times$  10 $^6$  EVs for every 30,000 HMSCs. 48 h post transfection, total protein was extracted from the cells, concentration determined by BCA assay (Thermo Scientific assay kit) and the luciferase activity from equal amounts of protein for each sample from each group was measured (reporter kit Promega) and normalized to control activity. The data is represented as mean% increase in luciferase activity ( $\pm$ SD,  $n = 4$ ) w.r.t control cells expressing the SMAD1/5 reporter. For the western blotting experiments, 100,000 HMSCs were cultured in 6 well plates and treated with 250 ng/ml rhBMP2, control EVs or BMP2 FEEs (20  $\times$  10 $^6$  particles). Each experiment was performed in triplicate. Four hours post treatment, the total protein from the cells was isolated and 20  $\mu$ g of protein from each group (estimated using the BCA assay kit from Thermo Scientific) was resolved by SDS PAGE followed by western blotting for phosphorylated SMAD 1/5/8 (1/250, Abcam) and tubulin (1/2000, Sigma). For quantitative analysis of SMAD phosphorylation, an in-cell western was performed. For this experiment, 10,000 HMSCs/well were seeded in 96 well plate and the same experiment was performed. The BMP2 and EV amounts were adjusted accordingly as per cell number. Each experiment contained 5 replicates. Four hours post treatment, the cells were fixed, permeabilized and immunostained for phosphorylated SMAD 1/5/8 and tubulin with the corresponding secondary antibodies and imaged using a Licor Odyssey CLX imager. The fluorescence within the wells was quantitated using the image analysis software (Image Studio) provided with the instrument. The results were normalized to tubulin expression.

## 2.7. SMURF1 expression studies

100,000 HMSCs were cultured in 6 well plates and treated with BMP2 FEEs (20  $\times$  10 $^6$  particles). Untreated cells served as control. Each experiment was performed in triplicate. 48 h post treatment, the total protein from the cells was isolated and 20  $\mu$ g of protein from each group (estimated using BCA assay kit from Thermo Scientific) was resolved by SDS PAGE followed by western blotting for SMURF1 (Santa Cruz 1/500) and tubulin (loading control, 1/2000 Sigma) with the corresponding secondary antibodies and imaged using a Licor Odyssey CLX imager.

## 2.8. Argonaute 2 (AGO2) knockdown (AGO2 KD) and SMAD 1/5/8 phosphorylation

AGO2 was silenced by lentiviral mediated transduction of AGO2 shRNA in HMSCs (Santa Cruz Biotechnology). Silencing was verified by immunoblotting with the AGO2 antibody (1/250, Abcam). Control and AGO2 KD HMSCs were subjected to in-cell western SMAD 1/5/8 phosphorylation assay as described under Section 2.6.

## 2.9. Quantitative miRNA expression in EVs

qRT PCR was used to evaluate the expression level of miRNAs in the exosomes. The miRNA was isolated from equal numbers of control and BMP2 EVs using the Qiagen miRNA isolation kit as per the manufacturer's protocol. cDNA synthesis was performed using the miScript II kit (Qiagen) and qRT PCR was performed using the SYBR Green PCR kit (Qiagen) using custom primers for the selected miRNA (Table 1). The primer specificity was verified by analyzing the melt curve of the amplified product for a single peak. As there is no defined housekeeping miRNA for EVs to standardize, direct quantitation was performed by utilizing exact amounts of small RNA from equal numbers of EVs for all groups for cDNA synthesis

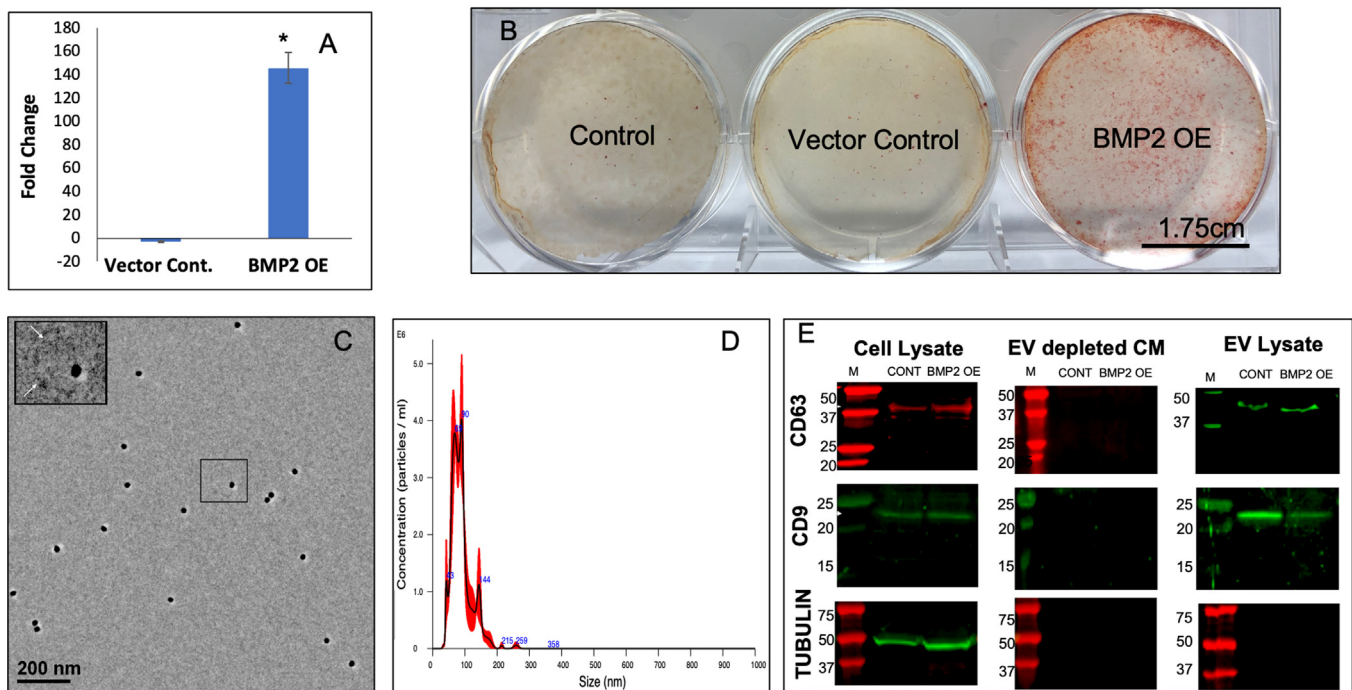


**Fig. 1.** Generation, isolation and characterization of BMP2 FEEs: A) Graph representing the fold change in the expression levels of BMP2 gene in vector control and BMP2 OE HMSCs with respect to untreated controls. Data represent mean foldchange  $\pm$  SD of three independent cultures. B) Representative images of alizarin red stained culture dishes of control, vector control and BMP2 OE HMSCs after 7 days of culture in osteogenic differentiation media. Scale bar represents 1.75 cm. Note the increase in calcium deposits in the BMP2 OE HMSC group. C) Representative TEM image of BMP2 FEEs immunolabeled for CD63 (20 nm gold dots). The insert represents the boxed area. The arrows in the insert represent the EV membrane. D) Representative NTA plot of BMP2 FEEs indicating exosomal size distribution. E) Immunoblots of Cell lysates, EV depleted conditioned medium and EV lysates from control and BMP2 OE HMSCs for the presence of CD63 and CD9 exosomal marker proteins as well as for the intracellular protein control tubulin. Note the absence of the EV markers and tubulin in the EV depleted conditioned medium and the absence of tubulin in the EV lysates.

**Table 1**

List of miRNA primer sequences used to measure expression levels in EVs.

miRNA	Primer sequence
has-miR15a-5p	GGGTAGCACGACATAATGGTTTG
has-miR15b-5p	GGGTAGCACGACATCATGGTTACA
has-miR16-5p	GGTAGCAGCACGTAATATTGGCG
has-miR424-5p	GGCACGAGCAATTATGTGTTGAA
has-miR497-5p	CAGCAGCACACTGTGGTTGT
has-miR3960	GCGGAGGGGGGGAAAAA

followed by quantitation of the cDNA amounts and double standardization to obtain the fold change in expression levels by using  $2^{-\Delta\Delta Cq}$  formula. The data is represented as mean fold change ( $n = 4$ ). Statistical significance was calculated between the control and BMP2 EV samples using student's *t*-test.

#### 2.10. Rat calvarial bone defect model

To evaluate the ability of FEEs to regenerate bone, a rat calvarial defect model was used. All animal experiments were performed in accordance with protocols approved by the UIC animal care committee (ACC, Assurance no: A3460.01). All groups and time points contained 6 defects per group. Briefly, the rats were anesthetized intraperitoneally using Ketamine (80–100 mg/kg)/Xylazine (10 mg/kg). Using aseptic technique, a vertical incision was made in the head at the midline to expose the calvarial bone. The connective tissue was removed and two 5 mm calvarial defects were created bilaterally in the calvarium without dura perforation using a trephine burr. A clinical grade collagen tape (Zimmer collagen tape) was placed on the wound with or without control or experimental EVs. The amount of EVs used was  $5 \times 10^8$  EVs per defect. Collagen tape alone served as control and rhBMP2

(50  $\mu$ g/wound, Medtronic) containing scaffolds served as positive control. The EV suspension (50  $\mu$ l volume) or rhBMP2 (50  $\mu$ l total volume) was loaded on to the collagen tape (25  $\mu$ l to each side of the tape) prior to placement on to the defect by adding it directly to the tape and allowing for adsorption on to the tape. Four, 8- and 12-weeks post-surgery, the rats were sacrificed by carbon dioxide asphyxiation followed by cervical dislocation. The calvaria were harvested, fixed in neutral buffered 4% paraformaldehyde and subjected to 3D  $\mu$ CT analysis using a Scanco40  $\mu$ CT scanner. The data obtained from the  $\mu$ CT scanner was quantitatively analyzed using a custom built MATLAB Program. The samples were then decalcified in 10% (w/v) EDTA solution, embedded in paraffin, and 10  $\mu$ m sections were subjected to H&E staining and immunohistochemistry (IHC) for BMP2 (1/250 Abcam), bone sialo protein (BSP, 1/250 Abcam), dentin matrix protein 1 (DMP1, 1/250, Santacruz Biotechnology) and osteocalcin (OCN, 1/250, Abcam).

#### 2.11. Statistical analysis

The normal distribution of the data obtained from the experiments was evaluated using the Shapiro-Wilk test. For experiments involving two groups, student's *t*-test with a confidence interval of 95% was utilized. For the experiments involving comparison of more than two groups, one-way ANOVA was performed with a confidence interval of 95%. Pairwise comparisons were performed using Tukey's ad-hoc test with a confidence interval of 95%.

### 3. Results

#### 3.1. Characterization of BMP2 OE HMSCs and BMP2 FEEs

Based upon earlier observations that lineage-specificity is imparted to HMSC EVs with a functional impact upon target

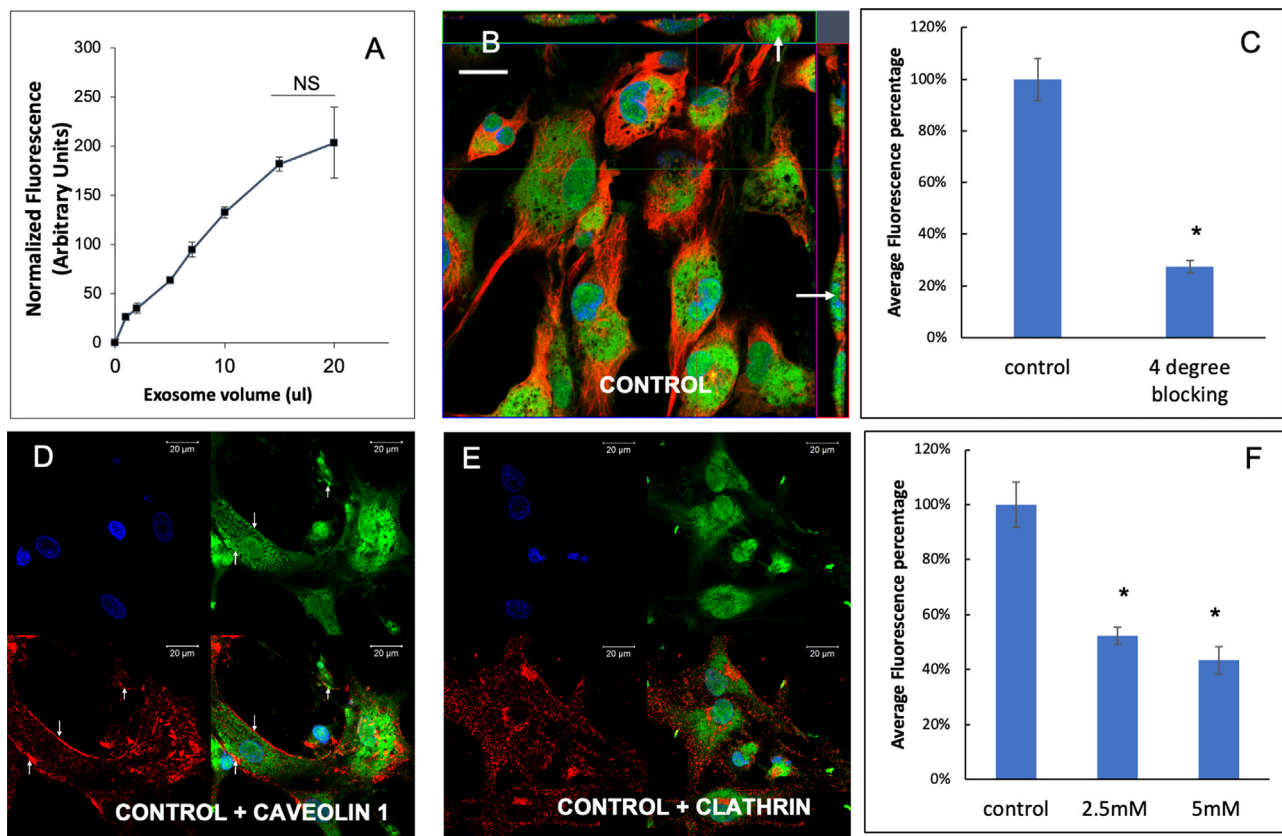


**Fig. 2.** Endocytosis of BMP2 FEEs by HMSCs: A) Graphical representation of dose-dependent and saturable endocytosis of fluorescently labeled BMP2 FEEs by naïve HMSCs. Data points represent mean fluorescence  $\pm$  SD ( $n = 6$ ). All data points were statistically significant as measured by Tukey's ad-hoc test post ANOVA with respect to the untreated control and with respect to adjacent data points except as indicated between the last two points. B) Representative confocal micrograph showing orthogonal view of a z-stack of confocal images of BMP2 FEE endocytosis by naïve HMSCs at 37 °C. The arrows point to localization of the fluorescently labeled FEEs within the cells. Scale bar represents 20  $\mu\text{m}$ . C) Graph showing the reduction in BMP2 FEE endocytosis at 4 °C compared to 37 °C (data represent mean percentage fluorescence  $\pm$  SD,  $n = 6$ ). \* represents statistical significance with respect to control as measured by student's *t*-test. D) Confocal micrograph showing colocalization of endocytosed BMP2 FEEs (green) with caveolin 1 (red). E) Confocal micrograph showing the absence of co-localization between endocytosed BMP2 FEEs (green) and clathrin (red). In images D and E, scale bar represents 20  $\mu\text{m}$ . F) Graph showing the reduction in HMSC endocytosis after disruption of target cell membrane cholesterol with increasing doses of MBCD. Data is presented as mean percentage fluorescence with respect to control  $\pm$  SD ( $n = 6$ ). \* represents statistical significance with respect to control as measured by Tukey's ad-hoc test post ANOVA. (For interpretation of the references to color in this figure legend, the reader is referred to the web version of this article.)

cells [16], we speculated that genetic manipulation of HMSCs to direct osteoinduction of the parental cell, could result in altered HMSCs that generate EVs with enhanced functionality for targeted osteoblastic differentiation of target stem cells. To explore this possibility and to investigate the potential of generating standardized EVs from a stabilized parental cell line, we generated a stable HMSC line that constitutively overexpresses BMP2 (BMP2 OE HMSCs). This cell line demonstrated increased mRNA expression of BMP2 compared to control (untreated) and vector control cell lines (Fig. 1A). This increased BMP2 expression was also associated with functional differentiation of the established BMP2 OE HMSC line. Fig. 1B shows a representative image of the control, vector control and BMP2 OE HMSCs subjected to cell culture in 6 well dishes in the presence of osteogenic differentiation media (7 days) and stained for alizarin red to identify calcium deposits. The BMP2 OE HMSCs generated greater amounts of calcium deposits compared to the controls indicating their greater osteogenic differentiation potential.

The EVs that were isolated from control and BMP2 overexpressing (BMP2 OE) cells were characterized qualitatively by transmission electron microscopy (TEM) and for size distribution by NTA. TEM analysis revealed spherical vesicles between 100–150 nm in size for both groups (Fig. 1C). NTA analysis indicated that the isolated EVs possess a size distribution consistent with exosomes

[20,22] (Fig. 1D). Immunoblot analysis indicated the presence of exosomal marker proteins CD63 and CD9 in both control MSC EVs and BMP2 FEEs lysates and their respective parental HMSC lysates, but not in the EV depleted conditioned medium (Fig. 1E). Immunoblotting for tubulin revealed tubulin presence in the cell lysate, but not in the EV lysate or the EV depleted conditioned medium (Fig. 1E). The data presented here indicate that the EVs may be primarily composed of exosomes. However, as the exosomes and other EVs have overlapping properties, we will refer to them as EVs throughout this article.

### 3.2. Endocytosis of BMP2 FEEs

Here, we evaluated the endocytic mechanism of BMP2 FEEs by target HMSCs. BMP2 FEE endocytosis by HMSCs was a dose dependent and saturable process (Fig. 2A). 3D confocal microscopy of HMSCs treated with fluorescently labeled BMP2 FEEs indicated the presence of the endocytosed EVs within the cells (Fig. 2B). When quantitative endocytosis experiments were performed using saturable amounts of BMP2 FEEs at 4 °C, EV endocytosis was significantly blocked indicating the temperature and thereby, the energy dependency of the process (Fig. 2C). Recent studies have shown that naïve HMSC EVs are endocytosed by target cells via the caveolar endocytic pathway [23]. We therefore investigated if the endocytic pathway of the derivative EVs from genetically modified HM-

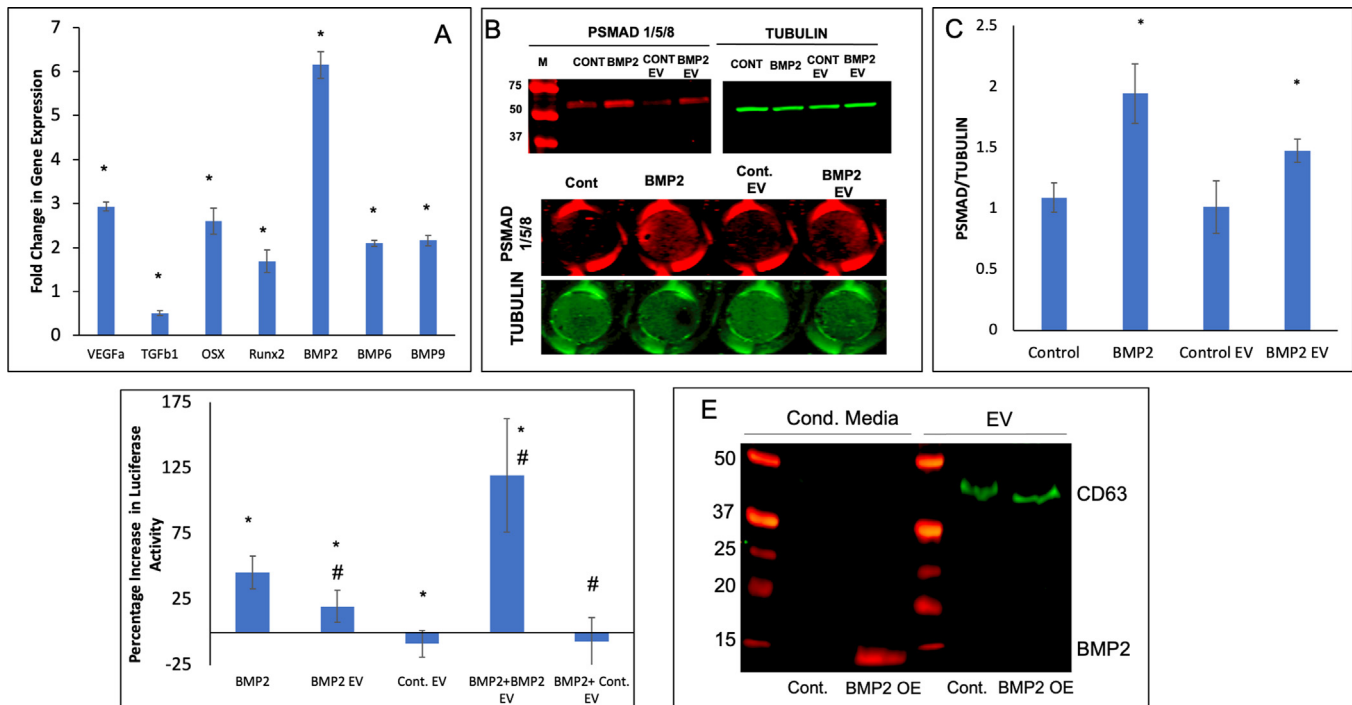


**Fig. 3.** BMP2 FEEs potentiate the BMP2 signaling cascade: A) Fold change in osteogenic gene expression (w.r.t untreated control) after HMSCs were treated with BMP2 EVs ( $1 \times 10^8$  EVs per 250,000 cells) for 72 h. \* Represents statistical significance w.r.t untreated control group ( $n = 4$ , student's *t*-test). B) Representative western blot ( $n = 3$ ) showing phosphorylated SMAD 1/5/8 (red lanes to the left) and tubulin (green to the right) after treatment of HMSCs with rhBMP2, Control EVs and BMP2 EVs. Note the increase in the band intensity for phosphorylated SMAD 1/5/8 after treatment with positive control BMP2 and with BMP2 EVs. For quantitation, an in-cell western was performed in 96 well plates ( $n = 5$ ). The image below the blots shows representative images of 96 well plates. C) Graphical quantitation of the intensity in each well for the in-cell western assay. \*represents statistical significance w.r.t control as measured by Tukey's ad-hoc pairwise test post ANOVA. Note that in line with the western blot data, the quantitative results show the phosphorylation of SMAD1/5/8 in the presence of BMP2 and BMP2 EVs. D) Graphical representation of SMAD 1/5 specific luciferase reporter assay that shows percentage increase in luciferase activity of the SMAD 1/5 specific reporter with the different treatments. Note the increase in activity after treatment with rhBMP2, BMP2 EVs and the combination of BMP2 and BMP2 EVs. \* represents statistical significance w.r.t untreated control and # represents statistical significance w.r.t the rhBMP2 treated group ( $n = 4$  for all groups) as measured by Tukey's ad-hoc pairwise test post ANOVA. E) Dual immunoblot for BMP2 (red) and CD63 (green) showing the presence of BMP2 in the EV-depleted conditioned medium from the BMP2 OE cells but not in the EV protein isolates of the control cell conditioned medium. CD63 was observed in the EV protein isolates only. (For interpretation of the references to color in this figure legend, the reader is referred to the web version of this article.)

SCs (BMP2 FEEs here) is affected as a result of the modifications to the parental cell. Colocalization experiments of HMSCs treated with fluorescently labeled FEEs with caveolin 1 and clathrin indicated that the endocytosed FEEs co-localize with caveolin 1 (Fig. 2D) and not with clathrin (2E) indicating the involvement of the caveolar endocytic pathway. Pretreatment of the recipient HMSCs with methyl  $\beta$  cyclodextrin (MBCD), a membrane cholesterol disruptor blocked BMP2 FEE endocytosis in a dose dependent manner, further confirming the involvement of the caveolar endocytic pathway (Fig. 2F). These results are similar to other studies of naïve and lineage-specified MSC derived EV endocytosis [18,19,23] and suggest that the BMP2 FEEs are endocytosed in a similar manner to MSC EVs isolated from naïve and differentiated states.

### 3.3. BMP2 FEEs enhance HMSC differentiation and BMP2 signaling in vitro

To explore whether the induced lineage-specification of HMSCs altered the function of the derivative EVs, we evaluated the potential of BMP2 FEEs to induce osteogenic differentiation of naïve HMSCs *in vitro*. BMP2 EV treated 3D HMSC cultures showed a significant increase in the expression of osteogenic marker genes including BMP2, RUNX2, osterix (OSX) and BMP9 (Fig. 3A). Based on the well-known effect of BMP2 signaling on osteogenic gene expression in HMSCs, we sought to evaluate if the EVs and FEEs themselves impact the BMP2 signaling cascade in target HMSCs. To test this, we examined SMAD1/5/8 phosphorylation in HMSCs that were subjected to a 4-h incubation with control EVs, BMP2

FEEs and with rhBMP2 (positive control). Untreated HMSCs were examined as baseline. Qualitative representative immunoblots and in-cell western results are presented in Fig. 3B for SMAD 1/5/8 phosphorylation. Fig. 3B shows representative 96-well images and the quantitation is provided in Fig. 3C ( $n = 5$ ). These results indicate that treatment with rhBMP2 and BMP2 FEEs triggered SMAD 1/5/8 phosphorylation. Treatment with control HMSC EVs did not increase SMAD 1/5/8 phosphorylation beyond resting cells state. To further evaluate the impact of EVs and FEEs on BMP2 signaling in target HMSCs, HMSCs were transfected with a reporter luciferase construct that is specific to SMAD 1/5 activity [21] and evaluated for signaling responses. The SBE12 luciferase activity was increased upon treatment with positive control BMP2 and to a lesser extent with BMP2 FEEs (Fig. 3D). When the EVs or FEEs were used in combination with rhBMP2, a robust increase in luciferase activity was observed with the BMP2 FEEs but not with control EVs indicating that the BMP2 FEEs were potentiating the BMP2 signaling cascade.

To exclude the possibility that BMP2 FEE effects were not the result of BMP2 protein present within the FEEs or contaminating the FEEs preparation, we examined both the FEEs and FEEs depleted conditioned media for BMP2 and EV marker CD63 expression. Fig. 3E shows that BMP2 protein was not present in detectable levels in the EV depleted conditioned medium of control cells. Importantly, BMP2 protein was also absent in the protein extracts from the control EV and BMP2 FEEs. As expected, BMP2 was detected in the EV depleted conditioned medium from the BMP2 OE HMSCs (red band in lane 2 of Fig. 3E). CD63 (green band) was

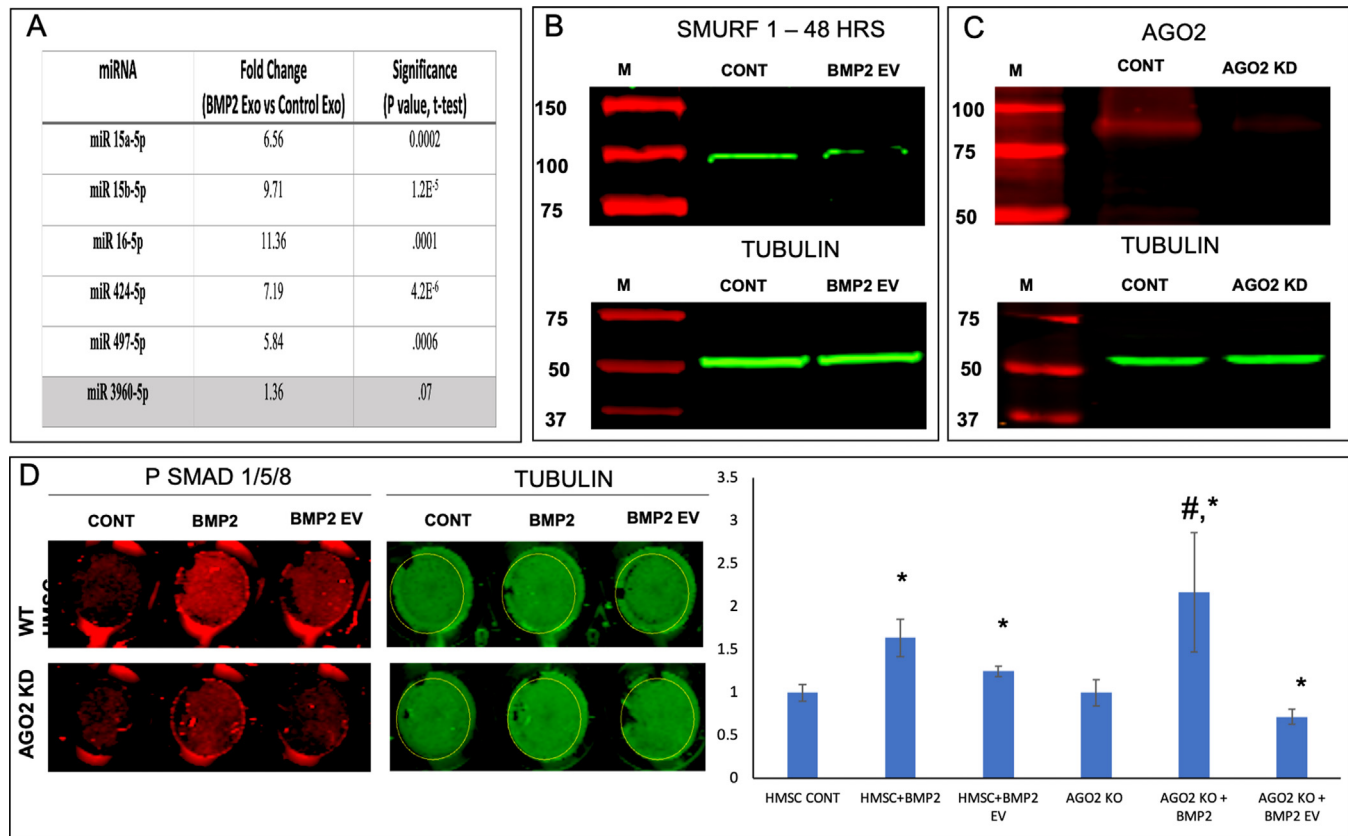


**Fig. 4.** Role of BMP2 FEE miRNAs: A) Table listing the mean fold change ( $n = 4$ ) in the expression levels of miRNA that bind to the 3'UTR of SMAD7 and SMURF1. miRNA 3960 is a pro-osteogenic miRNA that remained unchanged and is used as a control to show pathway specific increase in EV miRNA composition. P value was calculated using student's *t*-test. B) Immunoblot of SMURF1 in untreated control HMSC cell lysate and BMP2 EV treated cell lysate (top) and the corresponding tubulin blot (loading control, bottom). Note the reduction in the expression of SMURF 1 post treatment with BMP2 EVs. C) Immunoblot confirming the knockdown of AGO2 protein expression in HMSCs (top) and the corresponding tubulin loading control (bottom). D) Representative in-cell western images of wells representing PSMAD 1/5/8 (red) and tubulin (green) expression in control (WT HMSC) and AGO2 knockdown (AGO2 KD) HMSCs treated with rhBMP2 or BMP2 EVs. Note the reduction in the level of PSMAD 1/5/8 in the BMP2 EV treated AGO2 KD group compared to the WT HMSC group. The graph represents the quantitation of the in-cell western results ( $n = 5$ ). \*represents statistical significance w.r.t control and # represents statistical significance with respect to untreated AGO2 KD group as measured by Tukey's ad-hoc pairwise test post ANOVA. (For interpretation of the references to color in this figure legend, the reader is referred to the web version of this article.)

absent in the EV depleted media and present only in the EV protein extracts from both groups. Together, these findings indicated that BMP2 protein was not packaged within the FEEs of the BMP2 OE HMSCs.

We next sought to identify by a bioinformatic approach if an exosomal miRNA-based mechanism enables BMP2 FEEs to potentiate the BMP2 signaling pathway. To identify possible miRNA targets, we used TargetScan (targetscan.org) to identify miRNA targets that might bind to the negative regulators of the BMP2 pathway. We identified a cluster of five miRNAs that bind to the 3' untranslated region (UTR) of both SMURF1 and SMAD7. These miRNAs are broadly conserved among vertebrates. To evaluate if these miRNAs were differentially expressed among control and BMP2 EVs, the miRNA levels in control EVs and BMP2 FEEs were analyzed by qRT PCR. We observed a statistically significant increase in the levels of these miRNA in the BMP2 FEEs compared to control HMSC EVs (Fig. 4A). There are other miRNAs that control osteoinduction, however, here we observed by example that there was no significant change in the expression level of miRNA 3960, an miRNA implicated in osteogenic differentiation and bone regeneration via regulation of RUNX2 gene [24].

When the protein lysates from untreated and BMP2 FEE treated HMSCs were analyzed for SMURF1 expression by immunoblotting, a reduction in SMURF1 protein levels was observed (Fig. 4B). To further validate the role of EV miRNA, we knocked down AGO2

(AGO2 KD) in HMSCs by lentiviral transduction of AGO2 shRNA. AGO2 is a key protein involved in the formation of the RNA-induced silencing complex (RISC) that is necessary for miRNA activity. Fig. 4C confirms the reduction in protein levels of AGO2. When these cells were treated with BMP2 FEEs and evaluated for SMAD 1/5/8 phosphorylation, the effect of BMP2 FEEs was negated in the AGO2 cells compared to the controls (Fig. 4D). However, both the control and AGO2 KD cells responded positively to rhBMP2 stimulation indicating that the agonist-receptor pathway was not affected by AGO2 knockdown. Taken together, these results indicate a pathway-specific mechanism of action for the BMP2 FEEs that is likely mediated by the miRNAs.

#### 3.4. BMP2 FEEs can promote enhanced bone regeneration in vivo

We demonstrated the *in vivo* biological functionality and translational relevance of BMP2 FEEs in a rat calvarial defect model. Fig. 5A shows representative 3D reconstructed  $\mu$ CT images of rat calvaria after 4- and 12-weeks post wounding. For these experiments, rhBMP2 was used as a positive control. rhBMP2 induced a rapid and robust bone growth throughout the study period compared to the other groups. At this high, effective dose, bone formation obliterated the calvarial sutures and matured over time. Areas of ectopic bone formation was also observed (12-week group white arrow). The analysis of the calvaria of rats treated

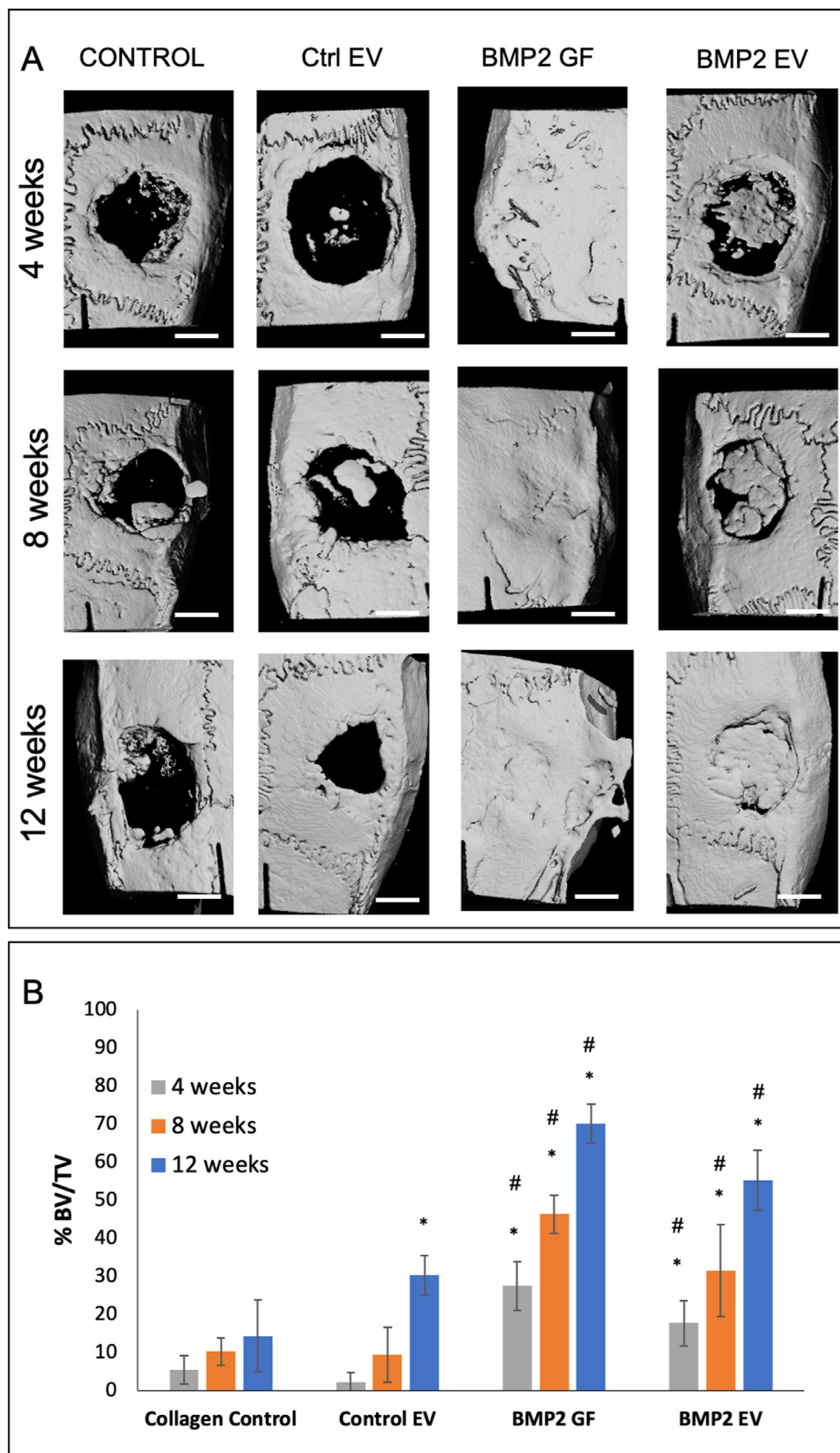


**Fig. 5.** BMP2 EV mediated bone regeneration: A) Representative  $\mu$ CT images showing regeneration of bone in 5 mm calvarial defects that were treated with plain collagen sponge (Control), collagen sponge containing control EVs (Ctrl. EV,  $5 \times 10^8$  EVs per defect), collagen sponge containing BMP2 (BMP2 GF  $5\mu\text{g}/\text{defect}$ ) and collagen sponge containing BMP2 EV ( $5 \times 10^8$  EVs per defect) at 4, 8- and 12-weeks post wounding. The arrow in the 12-week BMP2 GF group shows ectopic bone formation. Scale bar represents 2.5 mm. B) Volumetric quantitation of the  $\mu$ CT data expressed as percentage bone volume regenerated with mineralized tissue ( $n = 6$  defects per group per time point). \* represents statistical significance with respect to the collagen control group (no EV) and # represents statistical significance with respect to the control EV group. The significance was calculated using Tukey's ad-hoc test following one-way ANOVA.

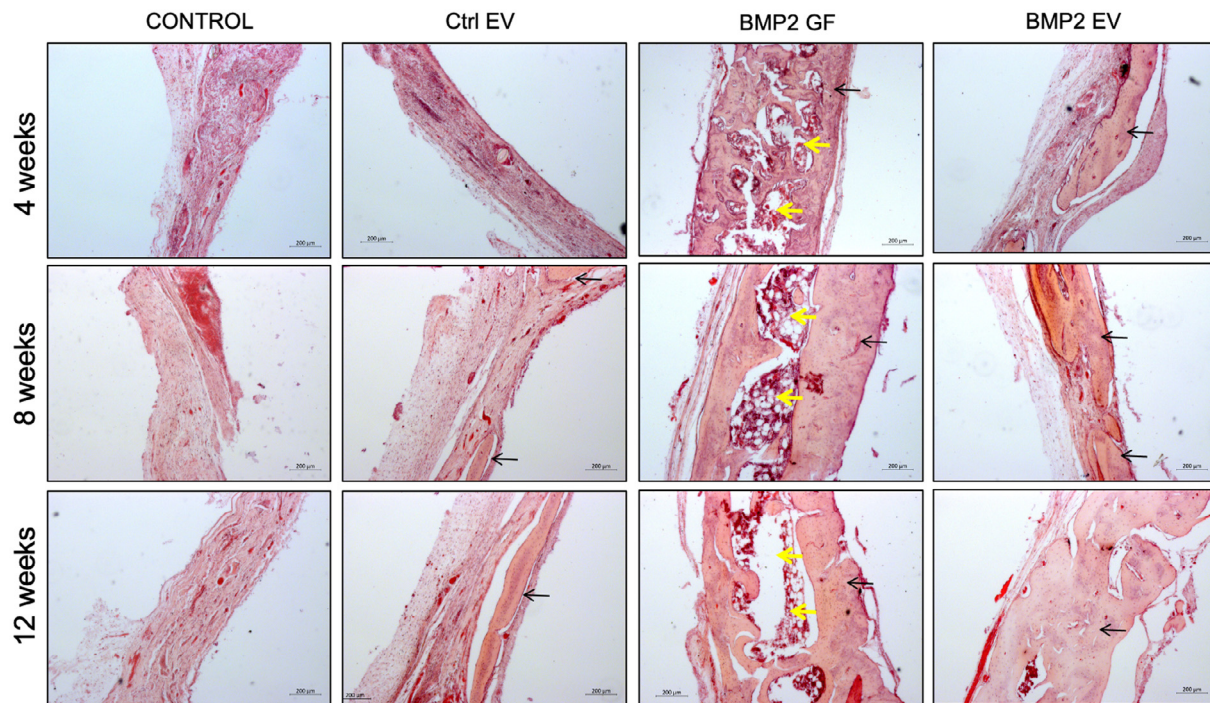


**Fig. 6.** Histological evaluation of calvarial defects: Images are representative light microscopy images of H&E stained demineralized calvarial samples of defects treated with plain collagen sponge (Control), collagen sponge containing control EVs (Ctrl. EV), collagen sponge containing BMP2 (BMP2 GF) and collagen sponge containing BMP2 EV after 4, 8- and 12-weeks post wounding. The black arrows in the images point to regenerated bone tissue. The yellow arrows in the BMP2 GF group point to fat deposits within the regenerated bone. Scale bar represents 200  $\mu$ m in all images. (For interpretation of the references to color in this figure legend, the reader is referred to the web version of this article.)

with BMP2 FEEs showed a gradual increase over time in bone formation that culminated in robust regeneration by 12 weeks. Mineralized bone formation appeared to be exclusively confined to the treated defect region. The control groups (no EV and control HMSC EV (Control EV)) showed minimal mineralized bone formation within the defects over the 12-week period. The  $\mu$ CT data was quantified using a custom designed MATLAB program that evaluates BV/TV ratios as percentage of defect volume filled with mineralized tissue at the different time points. In this program, the average radiopacity of the surrounding natural bone was used as the measure for determining bone within the defect area. The results of this quantification are presented in Fig. 5B and show that the healing of calvarial defects treated with BMP2 FEEs and rhBMP2 were significantly greater than the control group. The application of the BMP2 FEEs and rh BMP2 enhanced osseous regenerative function compared to EVs from naïve HMSCs.

Histological evaluation was performed on paraffin embedded sections of demineralized tissues across all groups and time points. Results presented in Fig. 6 validate the incomplete and poor healing observed in the control groups over the different time points evidenced by the increased presence of connective tissue and minimal bone matrix. In contrast, both the BMP2 FEE and the rhBMP2 groups displayed appreciable regeneration of bone tissue. The histological sections corroborate the  $\mu$ CT data indicating the comprehensive regeneration of bone tissue in the rhBMP2 group. However, a fatty marrow was observed in this group across all time points. This phenomenon has been reported previously by other groups and appears to be a side-effect of rhBMP2 treatment [8,25]. Notably, the BMP2 FEE group histology revealed ongoing woven bone formation across the defects, indicating a dedicated intramembranous bone regeneration process was induced.

Further, immunofluorescence staining was performed on the 4-week sections from the different groups to evaluate the ex-

pression levels of proteins important for bone formation. Results presented in Fig. 7 indicate that both rhBMP2 and the BMP2 FEE groups induced early expression of BMP2, bone sialoprotein (BSP), dentin matrix protein 1 (DMP1) and osteocalcin (OCN). Taken together, the  $\mu$ CT and histological results indicate that FEEs from a lineage-specified HMSC cell line (BMP2 OE HMSCs) are able to inform and target endogenous cells to differentiate along a parallel lineage to achieve tissue regeneration by a mechanism that enhances osteoinduction without intervening formation of fat, cartilage or other off target tissues.

#### 4. Discussion

Strategies aimed at bone regeneration should be effective in targeted differentiation of host MSCs with minimal immunological complications as well as reduced ectopic effects, but should possess efficacy equal or exceeding autogenous bone grafting [26]. MSC EVs may achieve these stated goals. Recent studies have identified the immunomodulatory effects of MSC EVs and their role in improving repair and regeneration of tissues [27]. Furthermore, published studies have shown that MSCs can be genetically modified to increase EV production by altering the secretory pathway [28]. The immunomodulatory, angiogenic and regenerative potential of HMSC EVs is well documented [29–31]. Others and us have shown the potential of bone marrow derived HMSC EVs in bone regenerative applications [16,32,33] including in the presence of titanium implants [34].

In this study, we have provided insights into how MSC EVs with enhanced tissue-specific regenerative potential may be generated by modifications to parental MSCs. Osteogenic differentiation of naïve MSCs for 2–4 weeks results in the generation of EVs with enhanced osteoinductive potential [16]. However, the repeated culturing of MSCs under differentiation conditions raises questions of reproducibility of the FEEs produced and, from a translational per-

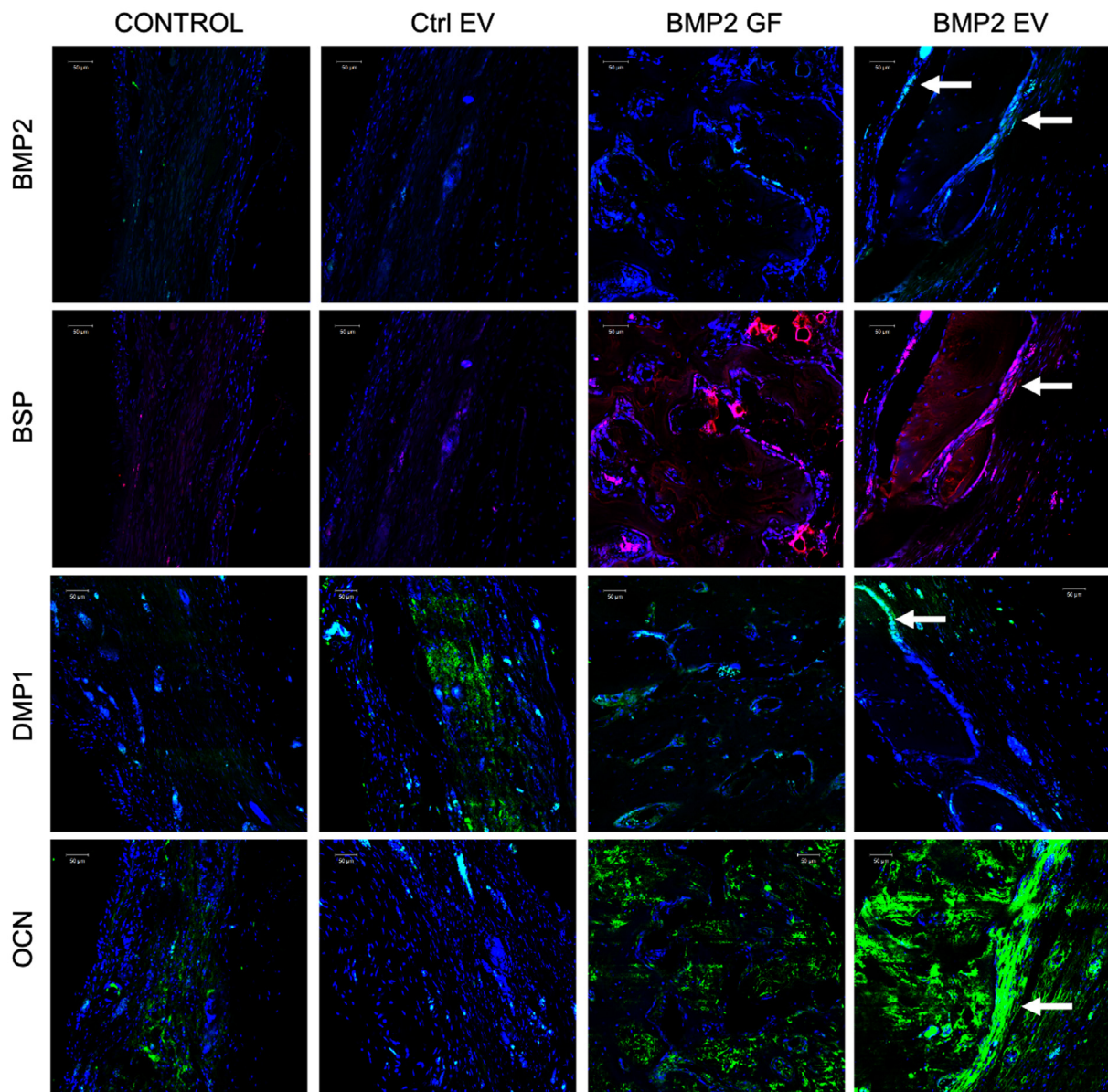


**Fig. 7.** IHC of calvarial defects: Images represent the expression levels of osteoinductive marker proteins BMP2, BSP, DMP1 and OCN in the calvarial sections from the different groups after 4 weeks. Note the increase in the expression levels of all markers in the rhBMP2 treated (BMP2 GF) and BMP2 EV treated groups. The arrows in the BMP2 EV group shows protein expression in the cells lining the newly formed bone. Scale bar represents 50 μm in all images.

spective, this approach is limited. Therefore, in this manuscript we sought to generate a genetically modified stable cell line that can consistently serve as a source of osteoinductive MSC EVs. We hypothesized that the stable transduction of HMSCs with an osteoinductive factor would generate a stable cell line that consistently produces osteoinductive EVs. To test this hypothesis, we generated an HMSC cell line that overexpresses BMP2. BMP2 is a clinically used morphogen for bone regenerative procedures in orthopedic and dental surgeries that is not without identified complications or side effects [25,35,36]. However, it is reproducibly efficient in the generation of bone in preclinical models including the model used here [37]. From this BMP2 overexpressing HMSC cell line, we obtained FEEs and characterized their physical, endocytic and functional properties.

We began by investigating the basic characteristics of the EVs from the BMP2 OE HMSCs. Results presented here indicate that EV

properties such as size distribution, PDI and EV marker expression remain unaltered as a result of genetic modification to the source cell. The ability of the FEEs to be endocytosed by naïve MSCs was investigated next. Characterization of the endocytic mechanism can be used to analyze if EV functional properties have been affected as a result of source cell modification. This is an important first step quality control assessment. Several different pathways including the clathrin and caveolar pathways (and in some cases non-classical pathways such as pinocytosis) have been identified as mode of EV endocytosis in different cell types [38–40]. The results presented here indicate that the BMP2 FEE endocytosis follows an unchanged mechanism of EV endocytosis and indicate that the basic EV properties have not been altered as a result of constitutive BMP2 expression in parental MSCs. Based on our prior studies with HMSC EVs and retinal tissues as well as EVs from the dental pulp MSCs, this appears to be a common endocytic mechanism

for MSC derived EVs [18,23]. Further studies using different MSC sources are required to conclusively determine if this mechanism is applicable to all MSCs in general.

When analyzed for their osteoinductive potential *in vitro*, BMP2 FEEs triggered an increase in the gene expression levels of osteoinductive growth factors (BMP2, BMP9) and transcription factors (RUNX2, OSX) in naïve HMSCs. Pathway studies indicated that the BMP2 FEEs potentiated the BMP2 signaling cascade. However, this potentiation was not due to BMP2 protein present within the EVs. We noted that the BMP FEEs alone resulted in modest increased BMP2 signaling and differentiation in the absence of exogenous BMP2 treatment. In the presence of BMP2, the BMP2 FEEs triggered a significant increase in pathway specific activity as measured by a SMAD1/5/8 specific reporter assay. These results suggest the possibility that BMP2 FEEs targeted innate inhibitors of the BMP2 signaling pathway thereby potentiating the effects of the signaling cascade.

Turning to a bioinformatic approach to identify possible miRNA targets that would represent such inhibitors, we identified SMURF1 and SMAD7 as potential miRNA targets possibly uniquely expressed in BMP2 FEEs. SMURF1 and SMAD7 are well characterized inhibitors of the BMP signaling pathway [41]. In fact, quantitative miRNA analysis of 5 miRNAs that target SMAD7 and SMURF1 were demonstrably upregulated in the BMP2 FEEs compared with HMSC EVs. Further studies by immunoblotting confirmed the reduction in SMURF1 expression upon treatment with BMP2 FEEs.

The miRNA dependent nature of BMP2 FEE action was affirmed by silencing of AGO2. In the relative absence of AGO2 expression, the ability of BMP2 FEEs enhance SMAD 1/5/8 phosphorylation was negated, but the BMP2 receptor mediated pathway remained unaffected. AGO2 is a key protein that is a part of the family of argonaute proteins involved in the formation of the RISC mediated gene silencing pathway [42]. While AGO1 is involved in the mRNA degradation pathway, AGO2 impairs mRNA translation directly [43]. Consistent with this role, we did not observe any changes in the mRNA levels of SMURF1 upon treatment with BMP2 FEEs, but a change in protein level was observed indicating the involvement of the AGO2 mediated pathway. Upon further literature review, we identified that one of the candidate miRs, miR-424, that showed increased expression in the BMP2 FEEs has been characterized by other groups for its role in downregulating SMURF1 and potentiating BMP2 signaling [44–46] suggesting a possible role in the observed effects. Conversely, it is possible that the observed result is a cumulative effect of multiple miRs culminating in enhanced functionality. Our studies have focused on the miRNA composition of the BMP2 EVs and its role in inducing osteogenic differentiation. However, EVs carry proteins as well as mRNAs. Therefore, it is possible that changes in EV protein and mRNA composition may contribute to BMP2 FEEs function. A robust miRNA Seq, proteomic and bioinformatics approach to understanding the full impact of engineered EVs and their role in stem cell differentiation is required. We anticipate that further refinement to EV engineering strategies using targeted expression of pathway-specific miRNA can enable changes to specified pathways and enhance therapeutic specificity and efficacy.

Here, we have employed the well-defined rat calvarial defect model to evaluate BMP2 FEE functionality *in vivo*. Based on  $\mu$ CT and histological comparisons, BMP2 FEEs promoted greater bone regeneration than control HMSC EVs. Apart from highlighting the enhanced potential of the FEEs, the data also revealed that EVs from undifferentiated HMSCs possess limited bone regenerative potential. This underscores the relative importance of an engineered EV strategy. While the BMP2 FEE group was qualitatively less robust than the group treated with 50  $\mu$ g/ml rhBMP2, the BMP2 FEE group did demonstrate nearly complete osseous wound healing within the 12-week period. The bone that was formed in

the BMP2 FEE group is representative of intramembranous woven bone. There was no evidence of ectopic or exaggerated bone formation, nor excessive vascular nor adipogenic tissue formation in this model.

The involvement of various cells and the targeting of individual cell types by BMP2 FEE treatment in this model remains to be elucidated and further studies are required to analyze the immunomodulatory effects of the BMP2 FEEs in comparison with control HMSC EVs. In addition, the various molecular mechanisms triggered by the BMP2 FEEs *in vivo*, the effects on angiogenesis and vascularization, as well as the changes to bone remodeling need careful investigation to broadly understand the underlying mechanisms. Collectively, the results from the bone regenerative experiments indicate that engineered EVs from genetically transformed HMSCs can be used as mediators of host response to injury to improve regenerative outcomes.

Overall, the present data indicate that EVs from genetically modified HMSCs (BMP2) were unaltered in size and endocytic properties compared to naïve HMSC EVs, yet showed enhanced regenerative potential *in vitro* and *in vivo* in line with the targeted genetic modification. This enhancement is due, in part, to altered EV cargo that includes miRNA that potentiates the BMP2 signaling cascade. These results show how properties of HMSC derived EVs may be manipulated for various applications in disease treatment and regenerative medicine. The translation of engineered EVs for clinical regeneration requires continued study of safety and feasibility and mass productivity. For example, viral transduction of host cells to overexpress growth factors has a possibility of potential negative side-effects. Scrutinizing of potential off-target effects is needed. Mass production of FEEs from engineered cell lines must be scalable, stable and efficient. By carefully studying and addressing these gaps in knowledge, the acknowledged role of EVs in wound healing can advanced using FEEs for use enhancing tissue repair and regeneration.

## Declaration of Competing Interest

The authors declare that they have no known competing financial interests or personal relationships that could have appeared to influence the work reported in this paper.

## Acknowledgment

This work was funded by NIH R01DE027404 and the Osteology foundation advanced researcher award (No: 17-106) to Ravindran and Gajendrareddy. We would like to acknowledge the support of the UIC research resources center (RRC) for their assistance with electron and confocal microscopy as well as for the NTA analysis.

## Supplementary materials

Supplementary material associated with this article can be found, in the online version, at doi:[10.1016/j.actbio.2020.04.017](https://doi.org/10.1016/j.actbio.2020.04.017).

## References

- [1] S. Gonnelly, C. Caffarelli, R. Nuti, Obesity and fracture risk, *Clin. Cases Miner Bone Metab.* 11 (1) (2014) 9–14.
- [2] N.B. Khazai, G.R. Beck Jr., G.E. Umpierrez, Diabetes and fractures: an overshadowed association, *Curr. Opin. Endocrinol. Diabetes Obes.* 16 (6) (2009) 435–445.
- [3] M.A. Flierl, W.R. Smith, C. Mauffrey, K. Irgit, A.E. Williams, E. Ross, G. Peacher, D.J. Hak, P.F. Stahel, Outcomes and complication rates of different bone grafting modalities in long bone fracture nonunions: a retrospective cohort study in 182 patients, *J. Orthop. Surg. Res.* 8 (2013) 33.
- [4] D.C. Smith, Extremity injury and war: a historical reflection, *Clin. Orthop. Relat. Res.* 473 (9) (2015) 2771–2776.

- [5] C. Marin, F.P. Luyten, B. Van der Schueren, G. Kerckhof, K. Vandamme, The impact of type 2 diabetes on bone fracture healing, *Front. Endocrinol.* 9 (2018) 6.
- [6] R. Langer, J.P. Vacanti, Tissue engineering, *Science* 260 (5110) (1993) 920–926.
- [7] M. Lykissas, I. Gkiatas, Use of recombinant human bone morphogenetic protein-2 in spine surgery, *World J. Orthop.* 8 (7) (2017) 531–535.
- [8] A.W. James, G. LaChaud, J. Shen, G. Asatrian, V. Nguyen, X. Zhang, K. Ting, C. Soo, A review of the clinical side effects of bone morphogenetic protein-2, *Tissue Eng. Part B Rev.* 22 (4) (2016) 284–297.
- [9] I. Ullah, R.B. Subbarao, G.J. Rho, Human mesenchymal stem cells – current trends and future prospective, *Biosci. Rep.* 35 (2) (2015) E00191.
- [10] Y.Z. Jin, J.H. Lee, Mesenchymal stem cell therapy for bone regeneration, *Clin. Orthop. Surg.* 10 (3) (2018) 271–278.
- [11] X. Liang, Y. Ding, Y. Zhang, H.F. Tse, Q. Lian, Paracrine mechanisms of mesenchymal stem cell-based therapy: current status and perspectives, *Cell Transpl.* 23 (9) (2014) 1045–1059.
- [12] A.I. Caplan, J.E. Dennis, Mesenchymal stem cells as trophic mediators, *J. Cell. Biochem.* 98 (5) (2006) 1076–1084.
- [13] M. Gnechi, Z. Zhang, A. Ni, V.J. Dzau, Paracrine mechanisms in adult stem cell signaling and therapy, *Circ. Res.* 103 (11) (2008) 1204–1219.
- [14] D.G. Phinney, M.F. Pittenger, Concise review: mSC-Derived exosomes for cell-free therapy, *Stem Cells* 35 (4) (2017) 851–858.
- [15] Y. Cui, J. Luan, H. Li, X. Zhou, J. Han, Exosomes derived from mineralizing osteoblasts promote ST2 cell osteogenic differentiation by alteration of microRNA expression, *FEBS Lett.* 590 (1) (2016) 185–192.
- [16] R. Narayanan, C.C. Huang, S. Ravindran, Hijacking the cellular mail: exosome mediated differentiation of mesenchymal stem cells, *Stem Cells Int.* 2016 (2016) 3808674.
- [17] Y. Qin, L. Wang, Z. Gao, G. Chen, C. Zhang, Bone marrow stromal/stem cell-derived extracellular vesicles regulate osteoblast activity and differentiation *in vitro* and promote bone regeneration *in vivo*, *Sci. Rep.* 6 (2016) 21961.
- [18] C.C. Huang, R. Narayanan, S. Alapati, S. Ravindran, Exosomes as biomimetic tools for stem cell differentiation: applications in dental pulp tissue regeneration, *Biomaterials* 111 (2016) 103–115.
- [19] C.-C. Huang, M. Kang, R. Narayanan, L.A. DiPietro, L.F. Cooper, P. Gajendrareddy, S. Ravindran, Evaluating the endocytosis and lineage-specification properties of mesenchymal stem cell derived extracellular vesicles for targeted therapeutic applications, *Front. Pharmacol.* 11 (163) (2020) E00163.
- [20] C. Thery, K.W. Witwer, E. Aikawa, M.J. Alcaraz, J.D. Anderson, R. Andriantsitohaina, A. Antoniou, T. Arab, F. Archer, G.K. Atkin-Smith, D.C. Ayre, J.M. Bach, D. Bachurski, H. Baharvand, L. Balaj, S. Baldacchino, N.N. Bauer, A.A. Baxter, M. Bebawy, C. Beckham, A. Bedina Zavec, A. Benmoussa, A.C. Beardi, P. Bergese, E. Bielska, C. Blenkiron, S. Bobis-Wozowicz, E. Boillard, W. Boireau, A. Bongiovanni, F.E. Borras, S. Bosch, C.M. Boulanger, X. Breakefield, A.M. Breglio, M.A. Brennan, D.R. Brigstock, A. Brisson, M.L. Broekman, J.F. Bromberg, P. Bryl-Gorecka, S. Buch, A.H. Buck, D. Burger, S. Busatto, D. Buschmann, B. Bussolati, E.I. Buzas, J.B. Byrd, G. Camussi, D.R. Carter, S. Caruso, L.W. Chamley, Y.T. Chang, C. Chen, S. Chen, L. Cheng, A.R. Chin, A. Clayton, S.P. Clerici, A. Cocks, E. Cocucci, R.J. Coffey, A. Cordeiro-da-Silva, Y. Couch, F.A. Coumans, B. Coyle, R. Crescitelli, M.F. Criado, C. D'Souza-Schorey, S. Das, A. Datta Chaudhuri, P. de Cardia, E.F. De Santana, O. De Wever, H.A. Del Portillo, T. Demaret, S. Deville, A. Devitt, B. Dhondt, D. Di Vizio, L.C. Dieterich, V. Dolo, A.P. Dominguez Rubio, M. Dominici, M.R. Dourado, T.A. Driedonks, F.V. Duarte, H.M. Duncan, R.M. Eichenberger, K. Ekstrom, S. El Andaloussi, C. Elie-Caille, U. Erdbrugger, J.M. Falcon-Perez, F. Fatima, J.E. Fish, M. Flores-Bellver, A. Forsonits, A. Frelet-Barrand, F. Fricke, G. Fuhrmann, S. Gabrielson, A. Gamez-Valero, C. Gardiner, K. Gartner, R. Gaudin, Y.S. Gho, B. Giebel, C. Gilbert, M. Gimona, I. Giusti, D.C. Goberdhan, A. Gorgens, S.M. Gorski, D.W. Greening, J.C. Gross, A. Guarneri, G.N. Gupta, D. Gustafson, A. Handberg, R.A. Haraszti, P. Harrison, H. Hegyesi, A. Hendrix, A.F. Hill, F.H. Hochberg, K.F. Hoffmann, B. Holder, H. Holthofe, B. Hosseinkhani, G. Hu, Y. Huang, V. Huber, S. Hunt, A.G. Ibrahim, T. Ikezu, J.M. Inal, M. Isin, A. Ivanova, H.K. Jackson, S. Jacobsen, S.M. Jay, M. Jayachandran, G. Jenster, L. Jiang, S.M. Johnson, J.C. Jones, A. Jong, T. Jovanovic-Talisman, S. Jung, R. Kalluri, S.I. Kano, S. Kaur, Y. Kawamura, E.T. Keller, D. Khamari, E. Khomyakova, A. Khorovor, P. Kierulf, K.P. Kim, T. Kislinger, M. Klingeborn, D.J. Klinke, 2nd, M. Kornek, M.M. Kosanovic, A.F. Kovacs, E.M. Kramer-Albers, S. Krasemann, M. Krause, I.V. Kurochkin, G.D. Kusuma, S. Kuypers, S. Laitinen, S.M. Langevin, L.R. Languiño, J. Lannigan, C. Lasser, I.C. Laurent, G. Lavieu, E. Lazaro-Ibanez, S. Le Lay, M.S. Lee, Y.X.F. Lee, D.S. Lemos, M. Lenassi, A. Leszczynska, I.T. Li, K. Liao, S.F. Libregts, E. Ligeti, R. Lim, S.K. Lim, A. Line, K. Linnemannstons, A. Llorente, C.A. Lombard, M.J. Lorenowicz, A.M. Lorincz, J. Lovatt, J. Lovett, M.C. Lowry, X. Loyer, Q. Lu, B. Lukomska, T.R. Lunavat, S.L. Maas, H. Malhi, A. Marcella, J. Mariani, J. Mariscal, E.S. Martens-Uzunova, L. Martin-Jaular, M.C. Martinez, V.R. Martins, M. Mathieu, S. Mathivanan, M. Maugeri, L.K. McGinnis, M.J. McVey, D.G. Meckes Jr., K.L. Meehan, I. Mertens, V.R. Minciucchi, A. Moller, M. Moller Jorgensen, A. Morales-Kastresana, J. Morhayim, F. Mullier, M. Muraca, L. Musante, V. Mussack, D.C. Muth, K.H. Myburgh, T. Najrana, M. Nawaz, I. Nazarenko, P. Nejsum, C. Neri, T. Neri, R. Nieuwland, L. Nimmerichter, J.P. Nolan, E.N. Nolte-t Hoen, N. Noren Hooten, L. O'Driscoll, T. O'Grady, A. O'Loghlen, T. Ochiya, M. Olivier, A. Ortiz, L.A. Ortiz, X. Osteikoetxea, O. Ostergaard, M. Ostrowski, J. Park, D.M. Pegtel, H. Peinado, F. Perut, M.W. Pfaffl, D.G. Phinney, B.C. Pieters, R.C. Pink, D.S. Pisetsky, E. Pogge von Strandmann, I. Polakovicova, I.K. Poon, B.H. Powell, I. Prada, L. Pulliam, P. Quesenberry, A. Radeghieri, R.L. Raffai, S. Raimondo, J. Rak, M.I. Ramirez, G. Raposo, M.S. Rayyan, N. Regev-Rudzki, F.L. Ricklefs, P.D. Robbins, D.D. Roberts, S.C. Rodriguez, E. Rohde, S. Rome, K.M. Roushop, A. Rughetti, A.E. Russell, P. Saa, S. Sahoo, E. Salas-Huenuleo, C. Sanchez, J.A. Saugstad, M.J. Saul, R.M. Schifefers, R. Schneider, T.H. Schoyen, A. Scott, E. Shahaj, S. Sharma, O. Shatnaya, F. Shekari, G.V. Shelke, A.K. Shetty, K. Shiba, P.R. Siljander, A.M. Silva, A. Skowronek, O.L. Snyder 2nd, R.P. Soares, B.W. Soda, C. Soekmadji, J. Sotillo, P.D. Stahl, W. Stoornvogel, S.L. Stott, E.F. Strasser, S. Swift, H. Tahara, M. Tewari, K. Timms, S. Tiwari, R. Tixeira, M. Tkach, W.S. Toh, R. Tomasini, A.C. Torrecillas, J.P. Tosar, V. Toxavidis, L. Urbanelli, P. Vader, B.W. van Balkom, S.G. van der Grein, J. Van Deun, M.J. van Herwijnen, K. Van Keuren-Jensen, G. van Niel, M.E. van Royen, A.J. van Wijnen, M.H. Vasconcelos, I.J. Vechetti Jr., T.D. Veit, L.J. Vella, E. Velot, F.J. Verweij, B. Vestad, J.L. Vinas, T. Visnovitz, K.V. Vukan, J. Wahlgren, D.C. Watson, M.H. Wauben, A. Weaver, J.P. Webber, V. Weber, A.M. Wehman, D.J. Weiss, J.A. Welsh, S. Wendt, A.M. Wheelock, Z. Wiener, L. Witte, J. Wolfram, A. Xagorari, P. Xander, J. Xu, X. Yan, M. Yanze-Mo, H. Yin, Y. Yuana, V. Zappulli, J. Zarubova, V. Zekas, J.Y. Zhang, Z. Zhao, L. Zheng, A.R. Zheutlin, A.M. Zickler, P. Zimmermann, A.M. Zivkovic, D. Zocco, E.K. Zubasurma, Minimal information for studies of extracellular vesicles 2018 (MISEV2018): a position statement of the international society for extracellular vesicles and update of the MISEV2014 guidelines, *J. Extracell Vesicles* 7 (1) (2018) 1535750.
- [21] K. Eguchi, Y. Akiba, N. Akiba, M. Nagasawa, L.F. Cooper, K. Uoshima, Insulin-like growth factor binding protein-3 suppresses osteoblast differentiation via bone morphogenetic protein-2, *Biochem. Biophys. Res. Commun.* 507 (1–4) (2018) 465–470.
- [22] R. Shah, T. Patel, J.E. Freedman, Circulating extracellular vesicles in human disease, *N. Engl. J. Med.* 379 (10) (2018) 958–966.
- [23] B. Mathew, S. Ravindran, X. Liu, L. Torres, M. Chennakesavalu, C.-C. Huang, L. Feng, R. Zelka, J. Lopez, M. Sharma, S. Roth, Mesenchymal stem cell-derived extracellular vesicles and retinal ischemia-reperfusion, *Biomaterials* 197 (2019) 146–160.
- [24] R. Hu, W. Liu, H. Li, L. Yang, C. Chen, Z.Y. Xia, L.J. Guo, H. Xie, H.D. Zhou, X.P. Wu, X.H. Luo, A runx2/mir-3960/mir-2861 regulatory feedback loop during mouse osteoblast differentiation, *J. Biol. Chem.* 286 (14) (2011) 12328–12339.
- [25] J.N. Zara, R.K. Siu, X. Zhang, J. Shen, R. Ngo, M. Lee, W. Li, M. Chiang, J. Chung, J. Kwak, B.M. Wu, K. Ting, C. Soo, High doses of bone morphogenetic protein 2 induce structurally abnormal bone and inflammation *in vivo*, *Tissue Eng. Part A* 17 (9–10) (2011) 1389–1399.
- [26] L. Cheng, K. Zhang, S. Wu, M. Cui, T. Xu, Focus on mesenchymal stem cell-derived exosomes: opportunities and challenges in cell-free therapy, *Stem Cells Int.* 2017 (2017) 6305295.
- [27] V. Borger, M. Bremer, R. Ferrer-Tur, L. Gockeln, O. Stambouli, A. Becic, B. Giebel, Mesenchymal stem/stromal cell-derived extracellular vesicles and their potential as novel immunomodulatory therapeutic agents, *Int. J. Mol. Sci.* 18 (7) (2017) E1450.
- [28] J. Phan, P. Kumar, D. Hao, K. Gao, D. Farmer, A. Wang, Engineering mesenchymal stem cells to improve their exosome efficacy and yield for cell-free therapy, *J. Extracell. Vesicles* 7 (1) (2018) 1522236.
- [29] R.C. Lai, F. Arslan, M.M. Lee, N.S. Sze, A. Choo, T.S. Chen, M. Salto-Tellez, L. Timmers, C.N. Lee, R.M. El Oakley, G. Pasterkamp, D.P. de Kleijn, S.K. Lim, Exosome secreted by msc reduces myocardial ischemia/reperfusion injury, *Stem Cell Res.* 4 (3) (2010) 214–222.
- [30] L.A. Reis, F.T. Borges, M.J. Simoes, A.A. Borges, R. Sinigaglia-Coimbra, N. Schor, Bone marrow-derived mesenchymal stem cells repaired but did not prevent gentamicin-induced acute kidney injury through paracrine effects in rats, *PLOS One* 7 (9) (2012) e44092.
- [31] A. Mokarizadeh, N. Delirezh, A. Morshedi, G. Mosayebi, A.A. Farshid, K. Marandi, Microvesicles derived from mesenchymal stem cells: potent organelles for induction of tolerogenic signaling, *Immunol. Lett.* 147 (1–2) (2012) 47–54.
- [32] X. Wang, O. Omar, F. Vazirisan, P. Thomsen, K. Ekstrom, Mesenchymal stem cell-derived exosomes have altered microRNA profiles and induce osteogenic differentiation depending on the stage of differentiation, *PLoS One* 13 (2) (2018) e0193059.
- [33] M. Martins, D. Ribeiro, A. Martins, R.L. Reis, N.M. Neves, Extracellular vesicles derived from osteogenically induced human bone marrow mesenchymal stem cells can modulate lineage commitment, *Stem Cell Rep.* 6 (3) (2016) 284–291.
- [34] X. Wang, F.A. Shah, F. Vazirisan, A. Johansson, A. Palmquist, O. Omar, K. Ekstrom, P. Thomsen, Exosomes influence the behavior of human mesenchymal stem cells on titanium surfaces, *Biomaterials* 230 (2020) 119571.
- [35] C.A. Tannoury, H.S. An, Complications with the use of bone morphogenetic protein 2 (BMP-2) in spine surgery, *Spine J.: Off. J. N. Am. Spine Soc.* 14 (3) (2014) 552–559.
- [36] K. Lee, E.A. Silva, D.J. Mooney, Growth factor delivery-based tissue engineering: general approaches and a review of recent developments, *J. R. Soc.: Interface* 8 (55) (2011) 153–170.
- [37] P.D. Mariner, J.M. Wudel, D.E. Miller, E.E. Genova, S.O. Streubel, K.S. Anseth, Synthetic hydrogel scaffold is an effective vehicle for delivery of infuse (rhBMP2) to critical-sized calvaria bone defects in rats, *J. Orthop. Res.* 31 (3) (2013) 401–406.
- [38] L.A. Mulcahy, R.C. Pink, D.R. Carter, Routes and mechanisms of extracellular vesicle uptake, *J. Extracell. Vesicles* 3 (2014) 3, doi:10.3402/jev.v3.24641.
- [39] C. Li, D.R. Liu, G.G. Li, H.H. Wang, X.W. Li, W. Zhang, Y.L. Wu, L. Chen, CD97 promotes gastric cancer cell proliferation and invasion through exo-

- some-mediated mapk signaling pathway, *World J. Gastroenterol.* 21 (20) (2015) 6215–6228.
- [40] F. Alcayaga-Miranda, M. Varas-Godoy, M. Khouri, Harnessing the angiogenic potential of stem cell-derived exosomes for vascular regeneration, *Stem Cells Int.* 2016 (2016) 11.
- [41] G. Murakami, T. Watabe, K. Takaoka, K. Miyazono, T. Imamura, Cooperative inhibition of bone morphogenetic protein signaling by smurf1 and inhibitory smads, *Mol. Biol. Cell* 14 (7) (2003) 2809–2817.
- [42] T. Kawamata, Y. Tomari, Making risc, *Trends Biochem. Sci.* 35 (7) (2010) 368–376.
- [43] U. Ghosh, S. Adhya, Non-equivalent roles of AGO1 and AGO2 in mRNA turnover and translation of cyclin D1 mRNA, *J. Biol. Chem.* 291 (13) (2016) 7119–7127.
- [44] L. Lu, M. Wu, Y. Lu, Z. Zhao, T. Liu, W. Fu, W. Li, MicroRNA-424 regulates cisplatin resistance of gastric cancer by targeting SMURF1 based on geo database and primary validation in human gastric cancer tissues, *Onco Targets Ther.* 12 (2019) 7623–7636.
- [45] R. Baptista, C. Marques, S. Catarino, F.J. Enguita, M.C. Costa, P. Matafome, M. Zuzarte, G. Castro, A. Reis, P. Monteiro, M. Pego, P. Pereira, H. Girao, MicroRNA-424(322) as a new marker of disease progression in pulmonary arterial hypertension and its role in right ventricular hypertrophy by targeting SMURF1, *Cardiovasc. Res.* 114 (1) (2018) 53–64.
- [46] X. Xiao, C. Huang, C. Zhao, X. Gou, L.K. Senavirathna, M. Hinsdale, P. Lloyd, L. Liu, Regulation of myofibroblast differentiation by miR-424 during epithelial-to-mesenchymal transition, *Arch. Biochem. Biophys.* 566 (2015) 49–57.